Materials Chemistry and Physics 125 (2011) 351–357

Contents lists available at ScienceDirect

Materials Chemistry and Physics

journal homepage: www.elsevier.com/locate/matchemphys

Fabrication of a room-temperature NO_2 gas sensor based on WO_3 films and WO_3/MWCNT nanocomposite films by combining polyol process with metal organic decomposition method

Pi-Guey Su*, Te-Tsun Pan

Department of Chemistry, Chinese Culture University, Taipei 111, Taiwan

ARTICLE INFO

Article history:
Received 10 May 2010
Received in revised form 22 October 2010
Accepted 2 November 2010

Keywords:
Polyol
Metal organic decomposition
Nanocomposite
Room-temperature sensor

ABSTRACT

Polyol process was combined with metal organic decomposition (MOD) method to fabricate a room-temperature NO_2 gas sensor based on a tungsten oxide (WO_3) film and another a nanocomposite film of WO_3/multi-walled carbon nanotubes (WO_3/MWCNTs). X-ray diffractometry (XRD), scanning electron microscopy (SEM) and atomic force microscopy (AFM) were used to analyze the structure and morphology of the fabricated films. Comparative gas sensing results indicated that the sensor that was based on the WO_3/MWCNT nanocomposite film exhibited a much higher sensitivity than that based on a WO_3 film in detecting NO_2 gas at room temperature. Microstructural observations revealed that MWCNTs were embedded in the WO_3 matrix. Therefore, a model of potential barriers to electronic conduction in the composite material was used to suggest that the high sensitivity is associated with the stretching of the two depletion layers at the surface of the WO_3 film and at the interface of the WO_3 film and the MWCNTs when detected gases are adsorbed at room temperature. The sensor that is based on a nanocomposite film of WO_3/MWCNT exhibited a strong response in detecting very low concentrations of NO_2 gas at room temperature and is practical because of the ease of its fabrication.

1. Introduction

Nitrogen oxides (NO and NO_2) generated by combustion facilities and automobiles are known to be extremely harmful to the human body and the environment. In particular, NO_2 is highly toxic to human nerves and respiratory organs, so highly sensitive detection is desired for monitoring air quality. Metal oxides are well known to be effective in detecting various gases with enough sensitivity. Among currently used metal oxides, WO_3 has been to be promising for NO_2 gas sensing applications [1–4], but it typically must usually be used at temperatures from 200 to 500 °C. At higher operating temperatures, the long-term stability of the metal oxide gas sensors drifts because oxygen vacancies in the metal oxides diffuse [5,6]. Therefore, a room-temperature gas sensor is important for monitoring nitrogen oxides for atmospheric environmental measurement and control.

Using nanostructured WO_3 as a gas-sensitive material has been widely studied in recent years, because such particles have large surface areas for the adsorption/desorption of gas molecules, and therefore are expected to improve gas-sensing performance. Therefore, several synthetic routes for preparing nanostructured WO_3, including aqueous alcoholic synthesis [7], thermal evaporation [8], sol–gel method [9,10], emulsion method and ion exchange method [11] and polyol method [12] have been used. Among these above methods, the polyol-mediated synthesis of materials is attractive, because the reaction conditions are easily established, and yield nano-sized particles in the form of dimensionally stable colloidal suspensions. Briefly, this approach uses a polyol with a high boiling point, including diethylene glycol, glycerol, glycol and others, as the reaction medium in the preparation of oxide materials. The polyols act as stabilizers, limiting particle growth and prohibiting agglomeration. Therefore, suitable reactants from homogenous solution (metal acetates/chlorides/alkoxides) are hydrolyzed at elevated temperature, forming nano-metal oxides/precursors in suspension in polyol [13–15].

Recently, organic–inorganic hybrid nanocomposite materials have attracted much interest in fundamental and applied research because of their potential commercial applications [16]. Carbon nanotubes (CNTs) exhibit very good adsorption properties because they have a high specific surface area and a nano-scale structure, which provides a large number of sites where gases can react [17]. The adsorption of gaseous molecules onto the surface of a CNT changes its electric properties, enabling the CNTs to act as gas sensors can be operated at room temperature [18,19]. Recently, composite films that are based on WO_3 nanopowders and multi-walled carbon nanotubes (MWCNTs) have been reported as new

* Corresponding author. Tel.: +886 2 28610511x25332; fax: +886 2 28614212.
E-mail address: spg@faculty.pccu.edu.tw (P.-G. Su).

0254-0584/$ – see front matter © 2010 Elsevier B.V. All rights reserved.
doi:10.1016/j.matchemphys.2010.11.001

gas sensitivity materials to reduce further the operating temperature and improve sensitivity [20,21]. One of the most used routes for preparing WO_3/MWCNT composite films is to mix WO_3 powder and MWCNTs with an organic vehicle to form a paste, which is then, usually deposited on a substrate as a sensitive film. However, MWCNTs lay among WO_3 grains, forming interface defects between WO_3 and MWCNTs in the composite film.

The metal organic decomposition (MOD) method for depositing a metal oxide thick film is easily and inexpensively applied [22,23]. Briefly, a metal alkoxide is spin-coated on a substrate, and then MOD forms a film of metal oxide. Tsai et al. [24–26] used the MOD method to prepare a SnO_2 film to detect amounts of alcohol and CO gases. In our previous study [27], SnO_2 and single-walled carbon nanotubes (SWCNTs) nanocomposite films were fabricated by the MOD method. However, no attempt has been made to produce a NO_2 gas sensor that is based on WO_3/MWCNTs nanocomposite films by combining the polyol process with the MOD method. In this work, WO_3/MWCNT nanocomposite films were fabricated by such a route, which has the advantages of being highly effective, inexpensive, and most importantly, suitable for industrial for mass production. In this approach, MWCNTs were added to the reaction medium to ensure that they were well-dispersed in the WO_3 matrix. The structural characteristics of the nanocomposite films were investigated by X-ray diffraction (XRD). The surface characteristics of the nanocomposite films were observed using atomic force microscopy (AFM) and scanning electron microscopy (SEM). The gas sensing properties of the nanocomposite films were tested using very low concentrations of NO_2. These structural and gas sensing characteristics were compared with those of WO_3 films obtained by the same fabrication process.

2. Experimental

2.1. Fabrication of gas sensors based on WO_3 films

Tungstic acid (H_2WO_4) (3.0 g) (99.9%, 5.59 g cm^{-3}, Merck) was added to 10 g of glycerol (99.5%, 1.259 g cm^{-3}, Merck) and the solution was heated to 190 °C for 1 h with vigorous magnetic stirring. The reaction can be easily followed by observing its distinctive color changes. Within minutes after the reaction's reaching 190 °C, the yellow solution turned pale green and then slowly changed to a deep blue suspension, indicating the formation of tungsten oxide nanoparticles in glycerol. The blue precursor was spin-coated on an alumina substrate with a pair of comb-like electrodes. Then, it was dried by heating to 170 °C in air for 2 h; MOD was then performed in a furnace at 400, 500, 600 and 700 °C for 4 h in the ambient atmosphere to form a film of WO_3. During the MOD process, the temperature was increased from the ambient temperature to the desired temperature at a heating rate of 5 °C min^{-1}. The thickness of the film was observed around 3 μm by SEM. Therefore, a gas sensor based on WO_3 film was obtained (Fig. 1).

2.2. Fabrication of gas sensors based on WO_3/MWCNT nanocomposite films

A surface-oxidized MWCNTs was prepared using the well established acid treatment [28] of MWCNTs that had been grown by raw chemical vapor deposition (CVD) (purity >95%, average diameter 110–170 nm, length about 5 μm, Aldrich Inc.) using an H_2SO_4/HNO_3 mixture (3:1, 50 ml), following by sonication at 80 °C for 3 h. The acid mixture was then decanted. The residue was then re-suspended in deionized water and centrifuged at 10,000 rpm for 30 min. This process was repeated many times until the solution pH was neutral, and was sonicated to facilitate a stable suspension of surface-oxidized MWCNTs in aqueous media.

Tungstic acid (H_2WO_4) (3.0 g) was added to 10 g of glycerol and the solution was heated to 190 °C for 1 h with vigorous magnetic stirring; the required amount of surface-oxidized MWCNTs was then added. The solution was continuously stirred until a stable suspension was obtained. The level of doping with surface-oxidized MWCNTs was varied among 0.01 wt.%, 1.0 wt.% or 1.7 wt.% (of H_2WO_4). The WO_3/MWCNTs nanocomposite films were formed by MOD in the same manner as in the fabrication of a gas sensor based on a WO_3 film. The MOD temperature was 500 °C for WO_3/MWCNT nanocomposite films.

2.3. Instruments and analysis

A Fourier Transform infrared spectrometer (FTIR, Nicolet 380) was used to obtain the IR spectra of the MWCNTs treated with acid. The surface microstructure of the WO_3 films and WO_3/MWCNT nanocomposite films coated on an alumina substrate was investigated using a field emission scanning electron microscope (FE-SEM, JEOL, JSM 6335F) and an atomic force microscope (AFM, Ben-Yuan, CSPM 4000) in tapping mode. The XRD powder pattern of the WO_3 films and WO_3/MWCNT nanocomposite films were measured using Cu Kα radiation (Shimadzu, Lab XRD-6000). The electrical and sensing characteristeristics were measured using a bench system at room temperature. Each sensor was connected in series with a load resistor and a fixed 5 V was continuously supplied to the sensor circuit from a power supply (GW, PST-3202). The resistance of the sensor was determined from the voltage at the ends of the load resistor using a DAQ device (NI, USB-6218) in various concentrations of gas. The desired NO_2 gas concentrations, obtained by mixing a known volume of standard NO_2 gas (1000 ppm) with air, were injected into the chamber. The cross-sensitivity experiment was performed by measuring the resistance of the sensor upon controlled concentration of 10, 10, 10, 10,000 and 100 ppm for NH_3, CO, C_2H_4, H_2 and C_2H_5OH gases, respectively. The gas inside the chamber was uniformly distributed using a fan. After some time, the chamber was purged with air and the experiment was repeated for another cycles. All experiments were performed at room temperature, and controlled the relative humidity to 40 RH%.

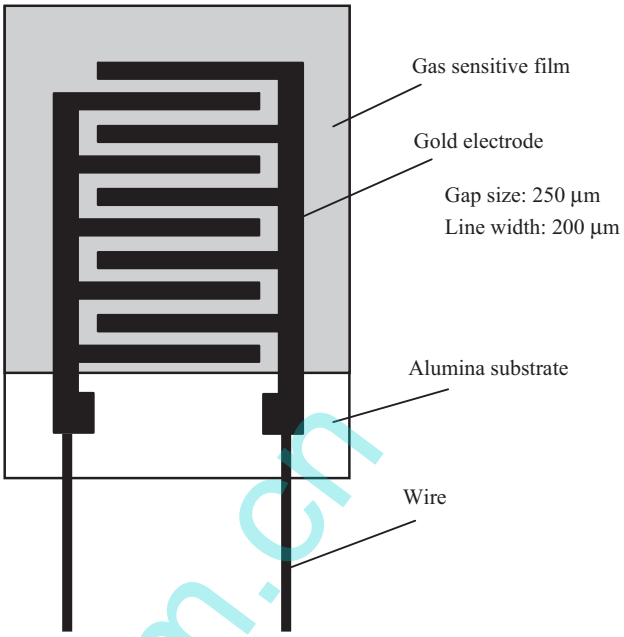

Fig. 1. Structure of NO_2 gas sensor.

3. Results and discussion

3.1. Precursor obtained from H_2WO_4

H_2WO_4 formed a yellow solution in glycerol. It subsequently turned pale green and then slowly turned into a deep blue suspension. Upon heating to 190 °C, the solution became pale green again. This phenomenon was similar to that observed by Jeyakumar and co-workers, who performed the polyol-mediated synthesis of WO_3 from dissolved WCl_6 in diethylene glycol [12], because W(VI) is a moderate oxidizing agent. Polyol reportedly acts as a reducing agent for noble metal ions [14]. Therefore, W(VI) was herein partially reduced to W(V) in polyol to yield a deep blue non-stoichiometric precursor. Polyol-mediated synthesis usually yields nanosized particles, and in this study yielded a colloidally stable blue suspension. Therefore, CNTs can be homogenously dispersed in a WO_3 matrix.

3.2. Structural characteristics of WO_3 films and WO_3/MWCNT nanocomposite films

3.2.1. XRD characterization

Fig. 2(a) shows the XRD spectra of the WO_3 films that were obtained by MOD at 400, 500, 600 and 700 °C. The XRD patterns of WO_3 films that were obtained by MOD at 400, 500, 600 and 700 °C all show three main peaks at $2\theta = 23.1$, 23.6 and 24.3°, which

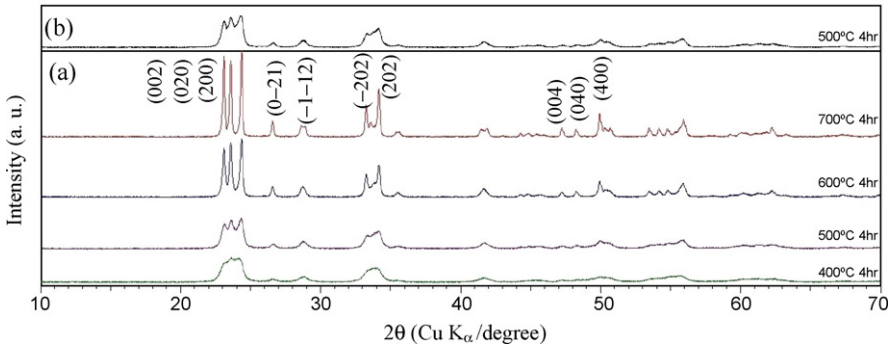

Fig. 2. XRD patterns of (a) WO_3 films and (b) WO_3/MWCNT nanocomposite film fabricated by polyol process and MOD.

are identified as corresponding to (0 0 2), (0 2 0) and (2 0 0) orientations, respectively. The XRD patterns of all samples showed the formation of monoclinic WO_3, as in the Joint Committee of Powder Diffraction Standards (JCPDS 00-020-1324) [29]. The diffraction peaks tended to be sharper as MOD temperature increased, indicating an increase in the particle size. Crystalline WO_3 was obtained after MOD at 400 °C for 4 h. Fig. 2(b) presents the XRD spectra of the WO_3/MWCNT nanocomposite films that were obtained by MOD at 500 °C for 4 h. Pure MWCNTs yielded a sharp peak that was centered at a 2θ value of 26°, corresponding to (0 0 2) planes [30]. However, no appreciable difference between the orientations and phases of WO_3 and WO_3/MWCNT samples was observed, because MWCNTs were embedded in the WO_3 matrix and so could not be easily detected by X-ray diffraction. The crystallite size of WO_3 and WO_3/MWCNT samples after MOD at various temperatures was estimated from XRD peaks according to Scherrer's equation:

$$D = \frac{0.9\lambda}{(B\cos\theta)} \quad (1)$$

where D represents mean grain size, B represents the full width at half maximum of the peak, λ is the wavelength of the X-rays, and θ is the angle of the center of the peak. The crystallite size was estimated from the half width of the (2 0 0) peak. Table 1 shows the estimated sizes of the grains of the WO_3 and WO_3/MWCNT samples. The grain size of the WO_3 samples increased from 14 to 65 nm as the MOD temperature increased. It did not detectably increase when MWCNTs were added to the WO_3 matrix.

3.2.2. AFM and SEM analyses

Fig. 3 presents the surface morphology of the WO_3 films and WO_3/MWCNT nanocomposite films that were prepared by the combined polyol and MOD method, determined using tapping-mode AFM. The size of each image is 5 μm × 5 μm. Table 2 presents the roughness and particle sizes of WO_3 films and WO_3/MWCNT nanocomposite films that were deposited on an alumina substrate at various MOD temperatures. Fig. 3(a)–(d) presents the surface morphologies of WO_3 films that were obtained by MOD at various temperatures. Fig. 3(a) shows the AFM image of the WO_3 film that was formed by MOD at 400 °C: it has a flatter surface than all of the others. Fig. 3(b) and (c) presents AFM images of WO_3 films that were formed by MOD at 500 and 600 °C, respectively. The surfaces of both films exhibit many islands that were dispersed among more uniformly sized particles over the whole scanned area. As the temperature increased to 700 °C (Fig. 3(d)), the sizes of the grains on the surface of the WO_3 film and the number of protuberances increased. The particle size and root mean square (RMS) roughness increased from 42 to 102 and from 7 to 59 nm, respectively, as the MOD temperature increased (Table 2). Fig. 3(e) presents the surface morphology of a WO_3/MWCNT nanocomposite film that was formed by MOD at 500 °C. A comparison with Fig. 3(b) reveals no obvious change in the particle size or RMS roughness of WO_3 when MWCNTs were added to the WO_3 matrix (Table 2).

Table 1
Grain size of WO_3 prepared by polyol process combined with MOD.

Annealing temperature (°C)	Grain size of WO_3 (nm)	Grain size of WO_3/MWCNT (nm)
400	14	–
500	27	28
600	48	–
700	65	–

Fig. 4 presents SEM images of the WO_3 films and the WO_3/MWCNT nanocomposite films that were formed by MOD at 500 °C. The WO_3 film exhibited a flat surface with many granules and some cracks (Fig. 4(a)). As presented in Fig. 4(b), no naked MWCNTs were present on the surface of the intentionally fractured WO_3/MWCNT nanocomposite film, even when the amount of added MWCNTs was increased to 1.7 wt.%. The MWCNTs were embedded in the WO_3 matrix and uniformly dispersed therein. The raw MWCNTs were treated with acid, and analyzed using an FTIR spectrometer, as presented in Fig. 5. The 1720 cm^{-1} peak may correspond to the stretching vibration mode of COOH (carboxylic group); the 1585 cm^{-1} peak to the asymmetric stretching vibration of the anion carboxylate ($-COO^-$) and the stretching of the C=C bond [28,31]. Chemical functional groups, –COOH, produced during vigorous acid treatment (chemical oxidation), enhancing the hydrophilic character of the MWCNTs, improving their MWCNTs dispersion in the WO_3 matrix. Evidently, the particle size and RMS roughness of the WO_3/MWCNT nanocomposite film were similar to those of the WO_3 film.

3.3. Gas sensing characteristics of WO_3 films and WO_3/MWCNT nanocomposite films

3.3.1. Gas sensing characteristics of WO_3 films

The sensor response (S) is given by $S = (R_{gas} - R_{air})/R_{air}$ ($\Delta R/R_{air}$), where R_{gas} and R_{air} are represent the electrical resistances of the sensor in the tested gas and air, respectively. Fig. 6 plots the response of the sensors based on WO_3 films that were prepared at various MOD temperatures toward NO_2 gas of 5 ppm at room temperature. Obviously, the response was strongly related to MOD temperature, and the film at 500 °C had the strongest response. Fig. 7 plots the responses of the sensor that was based on a WO_3 film that was prepared by MOD at 500 °C to various concentrations of NO_2 gas at room temperature. The electrical resistance of the WO_3 film increased when the film was exposed to NO_2 gas. The sensor did not respond to NO_2 gas at room temperature, except when the concentration exceeded 1 ppm, which result is consistent

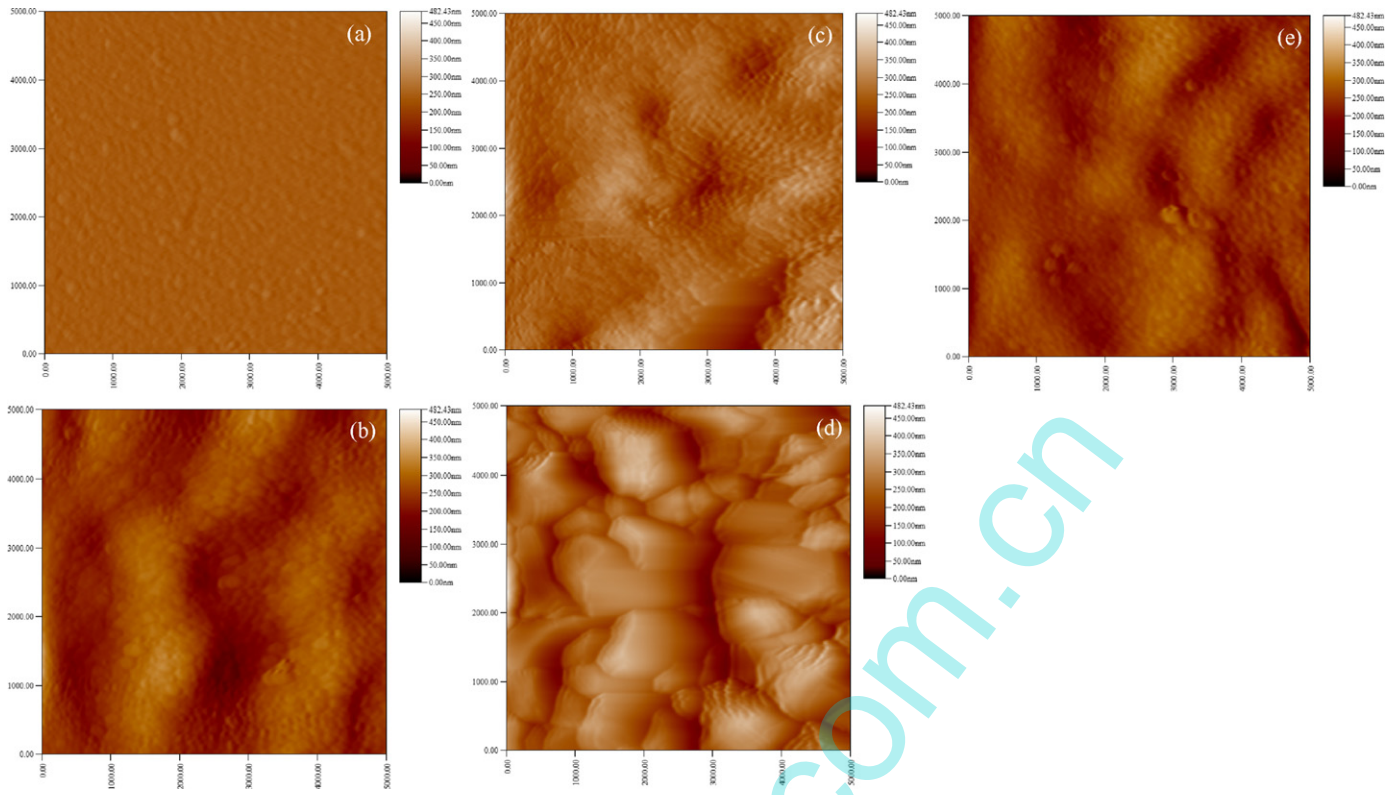

Fig. 3. AFM images of WO_3 films: (a)–(d) films formed by MOD at 400, 500, 600 and 700 °C, respectively; (e) WO_3/1.7 wt.% MWCNT nanocomposite film formed by MOD at 500 °C.

with results presented previously [20]. Fig. 8 plots the response (S) vs. concentration of NO_2 gas, for the sensor that was based on WO_3 film that was prepared by MOD at 500 °C. The sensitivity ($\Delta S/\Delta C$) is determined from the slope of the plot of response vs. gas concentration. The sensitivity and linearity (correlation coefficient, R^2) were 0.158 and 0.9609, respectively, at NO_2 gas concentrations in the range 5–20 ppm.

3.3.2. *Gas sensing characteristics of WO_3/MWCNT nanocomposite films*

The electrical resistance of the WO_3/MWCNT nanocomposite film increased when the film was exposed to NO_2 gas. Since NO_2 is an electron-withdrawing gas, the increase in the sensor resistance can be hypothesized as being caused by the fact that the composite sensing layer behaves as an n-type semiconductor. Fig. 9 plots the effect of the amount of added MWCNTs on the sensing properties of the WO_3/MWCNT nanocomposite films toward NO_2 gas at various concentrations of less than 1 ppm at room temperature. The electrical resistance of the WO_3/MWCNT nanocomposite films decreased as the MWCNTs loading increased, indicating that the new electrical paths in the WO_3 matrix were formed. The response (S) of the WO_3/MWCNT nanocomposite film to the addition of a small amount of MWCNTs (0.01 wt.% MWCNTs) was significantly stronger than that of the WO_3 film, suggesting that adding MWCNTs effectively enhanced the response to NO_2 gas at room temperature. The response (S) of a sensor that was based on WO_3/MWCNT nanocomposite film increased with the amount of added MWCNTs. The sensor that was based on a WO_3/1.7 wt.% MWCNT nanocomposite film exhibited the strongest response (S). The lowest detectable concentration was 100 ppb, at which the response value was 0.25. Therefore, the sensor that was based on WO_3/1.7 wt.% MWCNT nanocomposite film was further tested to evaluate its other gas sensing characteristics. The response time ($T_{res.90\%}$) is defined as the time required for the sensor to reach 90% of the maximum change in resistance following exposure to a given gas. The recovery time ($T_{rec.90\%}$) is defined as the time required for the sensor to recover 90% of the decrease in resistance after the sensor is exposed to a dry gas. Fig. 10 shows that the response ($T_{res.90\%}$) and recovery ($T_{rec.90\%}$) times of the sensor that was based on WO_3/MWCNT nanocomposite film were 10.5 and 20 min, respectively, at a testing concentration of NO_2 gas of 100 ppb. The response (S) vs. concentration of NO_2 gas for the sensor that was based on WO_3/MWCNT nanocomposite film that was prepared by MOD at 500 °C is also shown in Fig. 8. The sensitivity ($\Delta S/\Delta C$) is determined from the slopes of the plots of response vs. gas concentration. A steep decrease in the slope was observed at from 200 to 1000 ppb of NO_2 gas. Therefore, the sensitivity at 100–200 ppb NO_2 gas was higher than that at 200–1000 ppb. Fig. 11

Table 2
Roughness and particle size of WO_3 films and WO_3/MWCNT nanocomposite films deposited on alumina substrate.

Annealing temperature (°C)	WO_3 film		WO_3/MWCNT film	
	RMS (nm)	Particle size (nm)	RMS (nm)	Particle size (nm)
400	7	42	–	–
500	33	60	34	63
600	36	63	–	–
700	59	102	–	–

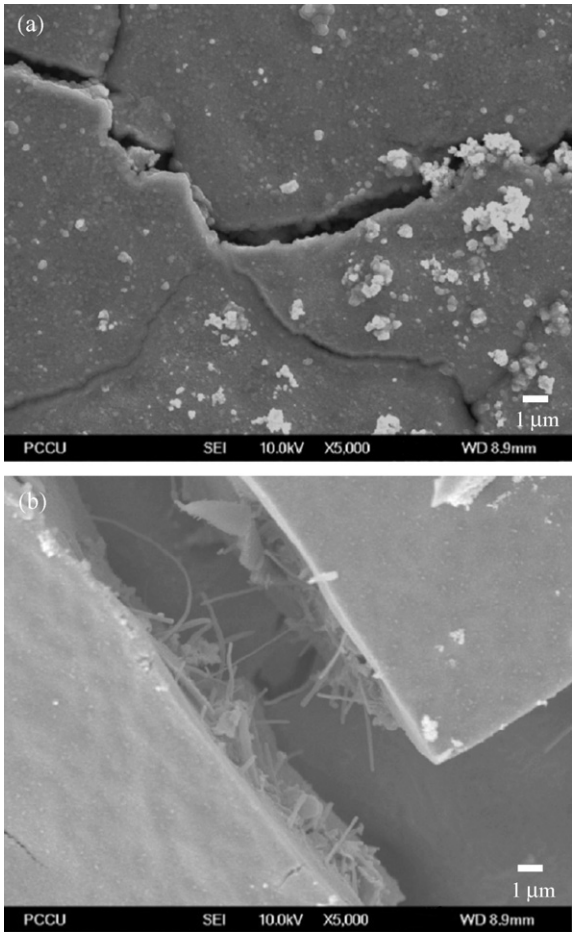

Fig. 4. FE-SEM images of (a) WO_3 film and (b) WO_3/1.7 wt.% MWCNT nanocomposite film formed by MOD at 500 °C.

plots the results concerning the cross-sensitivity effects of NH_3, CO, C_2H_4, H_2 and C_2H_5OH gases on the NO_2 gas sensor that was based on the WO_3/MWCNT nanocomposite film. NH_3, CO, C_2H_4, H_2 and C_2H_5OH gases may be regarded as having unobvious cross-sensitivity effects with NO_2 even at a low testing concentration of 200 ppb of NO_2. Fig. 12 plots the effect of ambient humidity on the response (S) of the sensor. A deviation of the response (S) of the sensor was observed when the ambient humidity exceeded 40% RH because the physisorbed water occupied the active sites of the sensing materials.

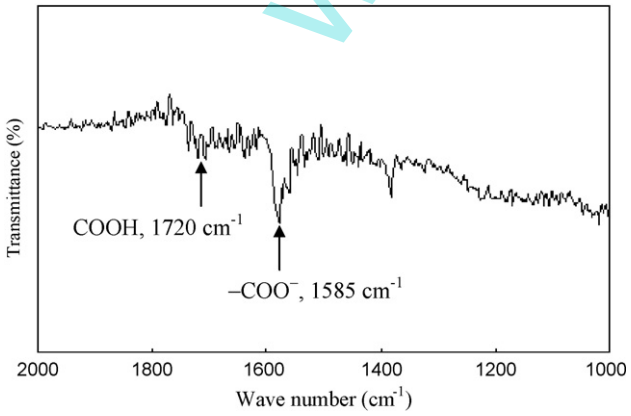

Fig. 5. IR spectra of MWCNTs treated with acid.

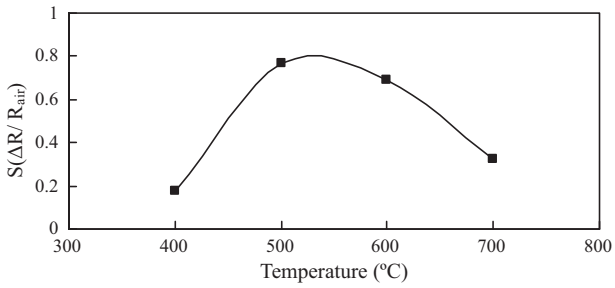

Fig. 6. Response of NO_2 gas sensors based on four WO_3 films that were prepared at various MOD temperatures to 5 ppm of NO_2 gas at room temperature.

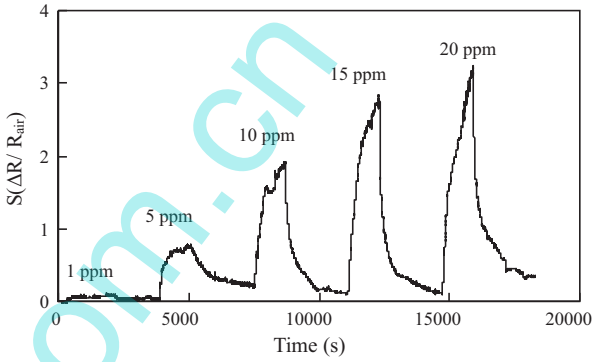

Fig. 7. Response curve of a NO_2 gas sensor based on WO_3 film formed by MOD at 500 °C as function of time (s) for various concentrations of NO_2 gas at room temperature.

3.4. Gas-sensing mechanism of sensor based on WO_3/MWCNT nanocomposite film

As described in Section 3.2, the surface morphology of the WO_3 film did not obviously differ from that of the WO_3/MWCNT nanocomposite film. Therefore, differences in surface morphology are not responsible for the much better sensitivity of the sensors that were based on WO_3/MWCNT nanocomposite film than that of the sensors that were based on WO_3 film. The issue can be analyzed by considering two main effects. First, the acid treatment of MWCNTs caused –COOH groups to attach to their surfaces

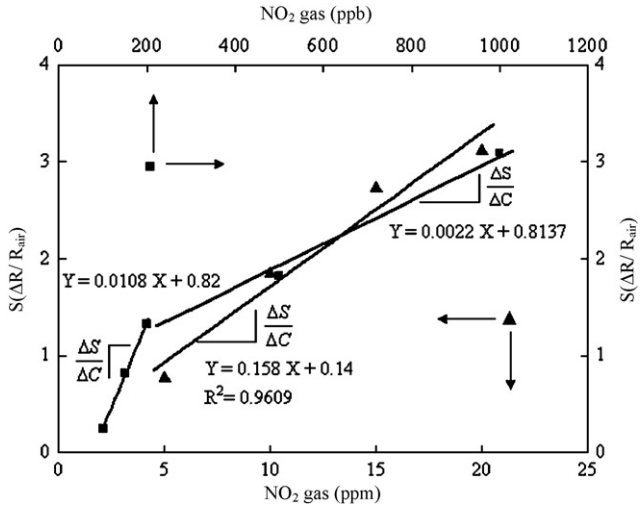

Fig. 8. Linear dependence of response of a NO_2 gas sensor based on (▲): WO_3 film and (■): WO_3/1.7 wt.% MWCNT nanocomposite film formed by MOD at 500 °C on concentration of NO_2 gas at room temperature. Sensitivity ($\Delta S/\Delta C$) is determined from the slope of the linear curve.

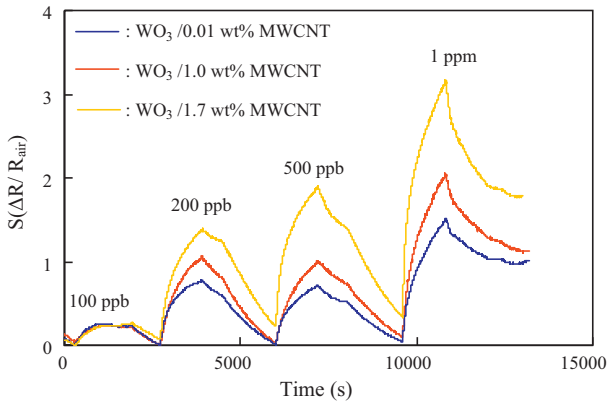

Fig. 9. Response curve of NO_2 gas sensor based on WO_3/MWCNT nanocomposite films formed by MOD at 500 °C as function of time (s) for various concentrations of NO_2 gas at room temperature.

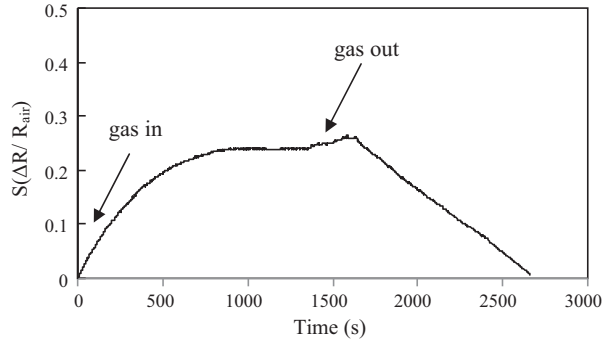

Fig. 10. Response curve of NO_2 gas sensor based on WO_3/1.7 wt.% MWCNT nanocomposite film formed by MOD at 500 °C on 100 ppb of NO_2 at room temperature.

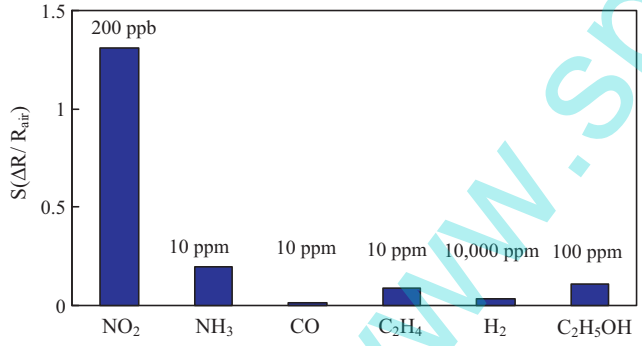

Fig. 11. Response (S) of the NO_2 gas sensor based on WO_3/1.7 wt.% MWCNT nanocomposite film formed by MOD at 500 °C to various gases.

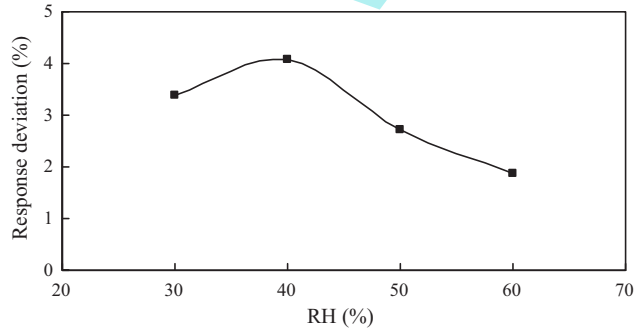

Fig. 12. Effect of ambient humidity on response of the NO_2 gas sensor based on WO_3/1.7 wt.% MWCNT nanocomposite film formed by MOD at 500 °C to 500 ppb of NO_2 gas at room temperature.

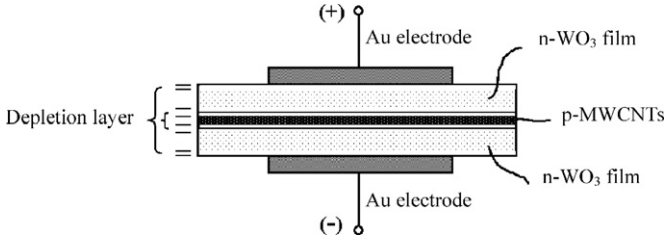

Fig. 13. Equivalent cross-sectional views of a NO_2 gas sensor based on WO_3/MWCNT nanocomposite film with hetero-structure (Au/n-WO_3/p-MWCNTs/n-WO_3/Au).

(Fig. 5). The increase in concentration of the functional groups is one of the main reasons for the increase in the electrical conductivity of the functionalized MWCNTs [32]. Therefore, new electrical paths in the WO_3 matrix were formed even with the addition of a small amount of MWCNTs. In this situation, the percolation effect is critical to electron transfer, and so the sensitivity of the WO_3/MWCNT nanocomposite film was better than that of the WO_3 film. Second, because the WO_3 matrix surrounds the MWCNTs, the p–n hetero-junction that was formed by MWCNTs and WO_3, which has been as indicated by Wei et al. [27] and Llobet and co-workers [20,21] must be considered. Since the WO_3 film behaved as an n-type semiconductor and the surface-oxidized MWCNTs film behaved as a p-type semiconductor [33], the hetero-structure Au/n-WO_3/p-MWCNTs/n-WO_3/Au formed at the interface between WO_3 and MWCNTs, as shown in Fig. 13. This hetero-structure is associated with the co-existence of two depletion layers (and associated potential barriers). The first depletion layer is located at the surface of the grains of the WO_3 film and the second is at the interface between the MWCNTs and the WO_3 film. The adsorption of NO_2 gas at the metal oxide modified the depletion layer at the surface of the WO_3 grains and in the n-WO_3/p-MWCNTs/n-WO_3 hetero-structures. Therefore, the gas was easily detected at room temperature, owing to the amplification effects of by the combination of the percolation effect and the junction structure of the WO_3/MWCNT nanocomposite film.

4. Conclusions

Room-temperature NO_2 gas sensors, based on WO_3 films and WO_3/MWCNT nanocomposite films, were successfully fabricated by combining polyol process with MOD. The crystalline structure, film morphology, and response to NO_2 of the WO_3 films and WO_3/MWCNT nanocomposite films were analyzed. The sensor based on the WO_3 film formed by MOD at 500 °C had a stronger response than those formed by MOD at other temperatures. The response of the WO_3/MWCNT nanocomposite films to NO_2 gas increased dramatically when a few MWCNTs were added to the WO_3 film. The sensor that is based on WO_3/1.7 wt.% MWCNT nanocomposite film was associated with the lowest detectable concentration (100 ppb). NH_3, CO, C_2H_4, H_2 and C_2H_5OH gases may be regarded as having unobvious cross-sensitivity effects with NO_2. However, the response/recovery time of the sensor was still long and an ambient humidity of over 40% RH caused cross-sensitivity effects in the detection of NO_2 at room temperature.

AFM, SEM and XRD analysis suggested that added of well-dispersed MWCNTs were embedded in the WO_3 film. Accordingly, the modulation of the width of two depletion layers at the surface of the WO_3 film and at the interface of the WO_3 film and MWCNTs, is postulated to explain the enhancement of the performance of the WO_3/MWCNT sensor over that of the pure WO_3 sensor.

Acknowledgement

The authors thank the National Science Council (Grant No. NSC 98-2113-M-034-001-MY2) of Taiwan for support.

References

[1] H.T. Sun, C. Cantalini, L. Lozzi, M. Passacantando, S. Santucci, M. Pelino, Thin Solid films 287 (1996) 258–265.
[2] C. Cantalini, H.T. Sum, M. Faccio, M. Pelino, S. Santucci, L. Lozzi, M. Passacantando, Sens. Actuators B 31 (1996) 81–87.
[3] Y.G. Choi, G. Sakai, K. Shimanoe, N. Miura, N. Yamazoe, Sens. Actuators B 95 (2003) 258–265.
[4] T. Kida, A. Nishiyama, M. Yuasa, K. Shimanoe, N. Yamazoe, Sens. Actuators B 135 (2009) 568–574.
[5] P.K. Clifford, D.T. Tuma, Sens. Actuators 3 (1983) 233–254.
[6] P.K. Clifford, D.T. Tuma, Sens. Actuators 3 (1983) 255–281.
[7] I. Jiménez, J. Arbiol, A. Cornet, J.R. Morante, IEEE Sens. 2 (2002) 329–335.
[8] A. Al Mohammed, M. Gillet, Thin Solid Films 48 (2002) 302–309.
[9] J. Shieh, H.M. Feng, M.H. Hon, H.Y. Juang, Sens. Actuators B 86 (2002) 75–80.
[10] V. Guidi, M. Blo, M.A. Butturi, M.C. Carotta, S. Galliera, A. Giberti, C. Malagu, G. Martinelli, M. Piga, M. Sacerdoti, B. Vendemiati, Sens. Actuators B 100 (2004) 277–282.
[11] Z. Lu, S.M. Kanan, C.P. Tripp, J. Mater. Chem. 12 (2002) 983–989.
[12] P. Porkodi, V. Yegnaraman, D. Jeyakumar, Mater. Res. Bull. 41 (2006) 1476–1486.
[13] C. Feldmann, Scripta Mater. 44 (2001) 2193–2196.
[14] C. Feldmann, C. Metzmacher, J. Mater. Chem. 11 (2001) 2603–2606.
[15] C. Feldmann, Adv. Funct. Mater. 2 (2003) 101–107.
[16] H.S. Nalwa, Handbook of Organic–Inorganic Hybrid Materials and Nanocomposites, Vol. 1 Hybrid Materials, American Scientific Publishers, 2003.
[17] P.G. Collins, K. Bradley, M. Ishigami, Science 287 (2000) 1801–1804.
[18] J. Kong, N.R. Franklin, C. Zhou, M.G. Chapline, S. Peng, K. Cho, H. Dai, Science 287 (2000) 622–625.
[19] O.K. Varghese, P.D. Kichambre, D. Gong, K.G. Ong, E.C. Dickey, C.A. Grimes, Sens. Actuators B 81 (2001) 32–41.
[20] C. Bittencourt, A. Felten, E.H. Espinosa, R. Ionescu, E. Llobet, X. Correig, J.J. Pireaux, Sens. Actuators B 115 (2006) 33–41.
[21] E.H. Espinosa, R. Ionescu, B. Chambon, G. Bedis, E. Scotter, C. Bittencourt, A. Felten, J.J. Pireaux, X. Correig, E. Llobet, Sens. Actuators B 127 (2007) 137–142.
[22] G.M. Vest, Mater. Res. Soc. Symp. Proc. 60 (1986) 35.
[23] P. Van Geloven, J. Moons, M. Honore, J. Roggen, Sens. Actuators 17 (1989) 361.
[24] P.P. Tsai, I.C. Chen, M.H. Tzeng, MRL Bull. Res. Dev. 6 (1992) 67–72.
[25] P.P. Tsai, I.C. Chen, M.H. Tzeng, Sens. Actuators B 13–14 (1993) 610–612.
[26] P.P. Tsai, I.C. Chen, M.H. Tzeng, Sens. Actuators B 24–25 (1995) 537–539.
[27] B.Y. Wei, M.C. Hsu, P.G. Su, H.M. Lin, R.J. Wu, H.J. Lai, Sens. Actuators B 101 (2004) 81–89.
[28] J. Zhang, H.L. Zou, Q. Qing, Y.L. Yang, Q.W. Li, Z.F. Liu, X.Y. Quo, Z.L. Du, J. Phys. Chem. B 107 (2003) 3712–3718.
[29] http://www.icdd.com/products/overview.htm.
[30] A. Cao, C. Xu, J. Liang, D. Wu, B. Wei, Chem. Phys. Lett. 344 (2001) 13–17.
[31] H.L. Hsu, J.M. Jehng, Y. Sung, L.C. Wang, S.R. Yang, Mater. Chem. Phys. 109 (2008) 148–155.
[32] C.H. Lau, R. Cervini, S.R. Clarke, M.G. Markovic, J.G. Matisons, S.C. Hawkins, C.P. Huynh, G.P. Simon, J. Nanopart. Res. 10 (2008) 77–88.
[33] R. Ionescu, E.H. Espinosa, E. Sotter, E. Llobet, X. Vilanova, X. Correig, A. Felten, C. Bittencourt, G. Van Lier, J.C. Charlier, J.J. Pireaux, Sens. Actuator B 113 (2006) 36–46.